ELSEVIER

Earth and Planetary Science Letters 169 (1999) 209–226

EPSL

www.elsevier.com/locate/epsl

Trace elements in anorthite megacrysts from the Kurile Island Arc: a window to across-arc geochemical variations in magma compositions

Ilya N. Bindeman [a,*,1], John C. Bailey [b]

[a] *Department of Geophysical Sciences, University of Chicago, 5734 S. Ellis Ave., Chicago, IL 60637, USA*
[b] *Institut for Petrology, Geologisk Institut, University of Copenhagen, Oster Voldgade 10, Copenhagen K, DK-1350, Denmark*

Received 2 October 1998; revised version received 25 March 1999; accepted 25 March 1999

Abstract

Anorthite megacrysts from twelve volcanic centers of the Kurile Island Arc were analyzed by the ion microprobe for concentrations of: Li, Be, B, F, Mg, P, Cl, K, Ti, Fe, Co, Rb, Sr, Y, Zr, Nb, Cs, Ba, La, Ce, Pr, Nd, Sm, Eu, and Pb. These 1–2-cm megacrysts are mainly found as early phenocrysts in basalts, but are also present in andesites, rhyolites and hybrid rocks from almost every studied volcanic center, both subaerial and submarine. Electron and ion microprobe studies show that the cores of these megacrysts are homogeneous and unzoned, whereas rims often result from overgrowth of sodium-richer plagioclase in equilibrium with its host, silica-richer melt. The cores of these megacrysts can be used to see back through fractional crystallization and magma mixing and serve as a 'window' into an earlier basaltic stage of magmatic evolution. Petrological observations and numerical crystallization modeling indicate that highly anorthitic plagioclase is the first or second (after olivine) liquidus phase in high-Al basalts regardless of varying K_2O contents across the arc.

Given the narrow compositional range of anorthite megacrysts, the across-arc chemical variations are well displayed by direct comparison of trace element concentrations in the megacrysts across the arc. The concentration of K in megacrysts increases linearly by a factor of 11; Ba, 13; Sr, Eu, 4; Be, Ti, P, 3; Li, 2, REE, 5–2; whereas concentrations of Pb, B and halogens and their ratios to HFSE either remain constant or decrease with deepening of the Benioff Zone from 110 to 220 km. We used ion microprobe-derived plagioclase–basalt partition coefficients to convert trace element concentrations in megacrysts to parental magmatic values. The reconstructed concentrations of several key trace elements and their correlation with Benioff Zone depth are consistent with whole-rock basalt data, but all give systematically more primitive compositions. Therefore, anorthite megacrysts are helpful for retrieving the chemistry of parental basalts which have subsequently suffered variable differentiation and mixing. They can be used to assess delicate variations in primary basaltic magma chemistry as a function of Benioff Zone depth. We also report new results for Sr, Nd and Pb isotopes for anorthite-bearing rocks and other rocks from the same volcanoes. Across-arc zoning with respect to trace element concentrations, ratios and isotopic values is largely linear and requires superposition of several petrogenetic processes: trace element transfer by fluids, variation in degree of partial melting and progressive change of the melting source.

Keywords: trace-element analyses; Kuril Islands; ion probe; partial melting; magmas

* Corresponding author. Tel.: +1 608 263 5659; Fax: +1 608 262 0693; E-mail: inbindem@midway.uchicago.edu
[1] Present address: Department of Geology and Geophysics, The University of Wisconsin–Madison, 1215 W. Dayton St., Madison, WI 53706, USA.

0012-821X/99/$ – see front matter
PII: S0012-821X(99)00086-2

1. Kurile Arc geochemical zoning

Across-arc geochemical zonation is the key to resolving the nature of magmatism at convergent margins [1,2]. The Kurile Island Arc constitutes one of the simplest natural laboratories where one can study subduction processes. Like other arcs, Kurile Arc volcanics display a pronounced and regular pattern of across-arc chemical variation not only with respect to K_2O but also to most trace elements, whereas along-arc variations are more subdued [3–6]. Subtle along-arc variations from the southern Kuriles to central and northern Kuriles have been noted and mostly attributed to the presence of the Sea of Okhotsk deep basin behind the southern Kuriles and the absence of such a deep basin behind the northern portion [3]. Magma chemistry changes from low-K, through medium-K to high-K series, corresponding to the deepening of the Benioff Zone from 110 to 220 km [6]. Reported Sr, Nd and B isotopic ratios show a decrease toward the rear arc [7–9]. Oxygen fugacity increases toward the rear arc [10], implying an increase in the water content of magmas. Magmatic volumes, however, decrease sharply from the volcanic front to the rear-arc. The relatively cold 80–110-Ma old Pacific Plate strikes the central part of the arc with head-on collision and this is responsible for the regular geometry of the subduction zone. In addition, there is little variation in the thickness and type of sediments being carried into the subduction zone along the arc [11,12] and the Pacific Plate is free of irregular features, such as microcontinents or volcanic plateaus.

In a comprehensive survey of submarine volcanoes using a combination of seismic reflection, deep-tow magnetometry and dredging, a long chain of submarine volcanoes in the rear-arc zone behind the Kurile Islands has been discovered (Fig. 1) [5,11]. Of the known 201 Quaternary (<2 Ma) volcanoes in the Kurile Island Arc, 96 are submarine [11]. The great majority of rear arc volcanoes are submarine (see Fig. 1) and were sampled by dredging.

The Benioff Zone beneath the Kuriles was remapped on the basis of a 20-year record of a comprehensive seismic network [13], and the depth of the Benioff Zone under each volcano is known within several kilometers of resolution: in the frontal zone it is 110–140 km and it deepens continuously to 160–220 km in the rear zone. This detailed geophysical knowledge can serve as a background to study the magnitude of across-arc geochemical variations and to assess different petrogenetic models of convergent margin magmatism.

2. Liquidus phase as a tool to measure the across-arc geochemical zoning

Studies of arc magma petrogenesis require an assessment of the conspicuous across-arc geochemical variations which reflect varying source compositions. In order to quantitatively assess the magnitude of such variations for each trace element, one needs to search for the most primitive mantle-equilibrated melts, or to compare early melts at the same stage of evolution.

Mantle-equilibrated basaltic melts with high Ni and Cr contents (e.g., [14,15]) (here referred to as 'primitive') are rare in island arcs. Such basaltic melts are parental to the more commonly observed siliceous rocks which result from fractional crystallization and/or AFC. Even basic rocks with SiO_2 < 55 wt% may represent ~50% fractionation, if clinopyroxene is a liquidus phase, because the major element composition of a clinopyroxene-bearing cumulate assemblage is not greatly different from that of basalt, its removal does not lead to a rapid melt fractionation. In contrast, crystallization of anorthitic plagioclase hallmarks rather primitive basalts. Crystallization of clinopyroxene prior to plagioclase rapidly decreases the Ca content of the melt, thereby preventing anorthitic plagioclase from forming (e.g., [16] and MELTS modeling below).

Besides the differentiation argument, it takes considerable effort to find primitive glassy basalts in arc setting (e.g., [14,17]). Even if primitive basaltic lavas are present within a volcano, they are often buried under thick layers of pyroclastics (e.g., silicic pumice and ignimbrites) which cover the whole volcano or even most of an island (e.g., Kunashir and Simushir). Lavas from the volcanic front are normally more differentiated than lavas from the rear arc, since the volcanic front is characterized by a thicker crust (e.g., Fig. 1). It is even more difficult to find primitive basaltic lavas by dredging methods.

The use of liquidus phases of a given composi-

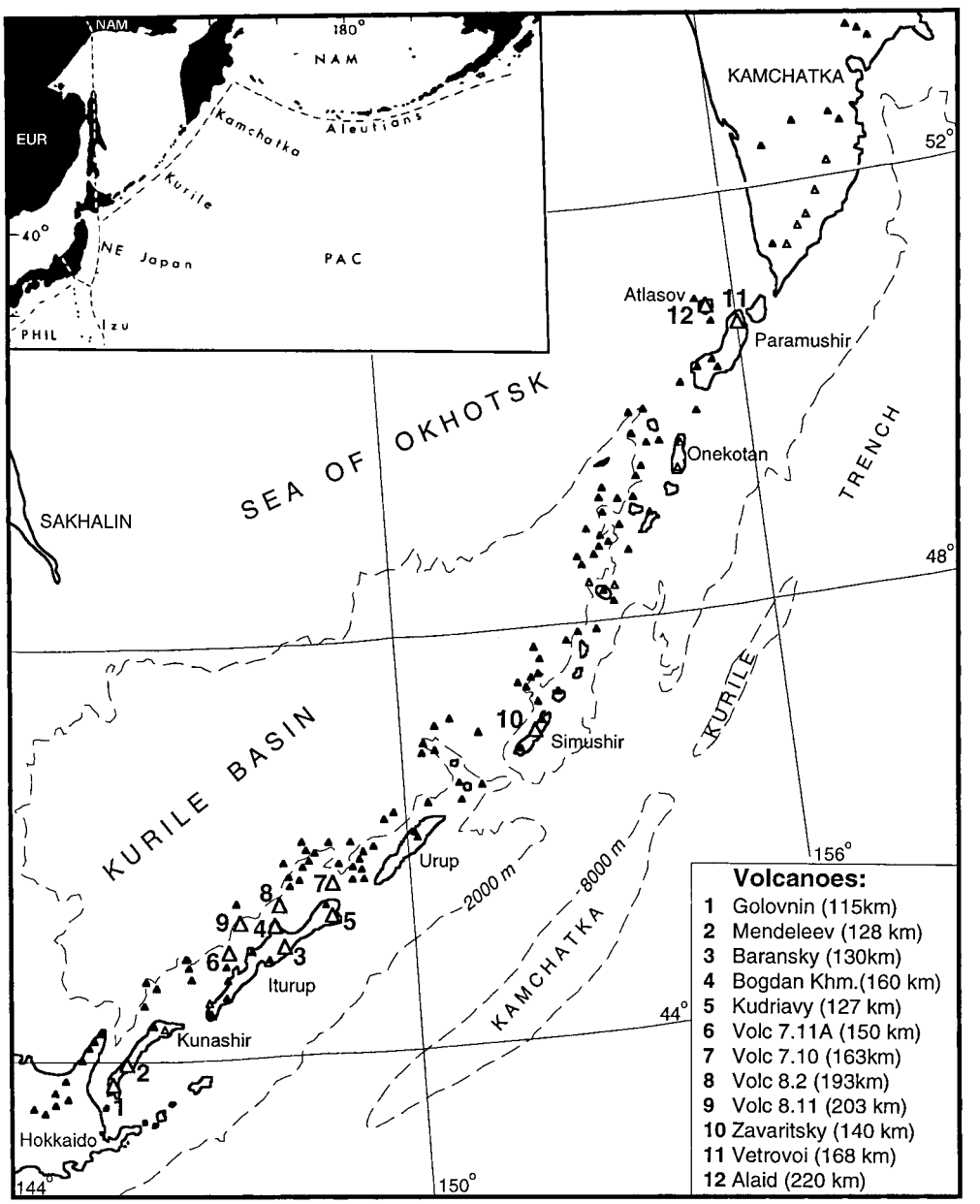

Fig. 1. Map of Kurile Island Arc with locations of studied samples (large triangles); numbers correspond to the order of volcanoes in Table 1 and to deepening of underlying Benioff Zone. Small triangles are other Quaternary volcanoes from [4]; open triangles denote volcanoes where anorthite megacrysts and/or anorthite–olivine cumulate inclusions have been found, based on authors' personal information and [11,22].

tion is an alternative way to measure the magnitude of across-arc geochemical variations. For example, when trace element concentrations in An_{90} plagioclase co-crystallizing with olivine of Fo_{80} compositions are compared across the arc, it can be assumed that the ranges of $P–T–X_{H_2O}$ parameters of An_{90}–Fo_{80} cotectic crystallization and pre-plagioclase differentiation history are similar across the arc.

In this work we present an ion microprobe study of the trace elemental composition of an early liquidus phase in these volcanics — anorthitic plagioclase megacrysts — as a 'window' to across-arc geochemical variations. We demonstrate that these megacrysts were crystallizing during a relatively primitive stage of basaltic magma fractionation and they, therefore, give insights into the petrogenetic processes beneath the arc. Note that plagioclase is the first liquidus mineral to contain measurable concentrations of trace elements of various geochemical groups (e.g., LILE, REE, HFSE).

In using plagioclase megacrysts it is assumed that the large and unzoned homogeneous Ca-rich cores preserve the original concentration of trace elements, inherited from the parental basaltic magma from which they crystallized. The ability of plagioclase to retain its original trace element composition is justified by the slow cation diffusion rates in plagioclase, which were shown to be the slowest among common minerals (e.g., olivines, pyroxenes, amphiboles) [18,19], and by their high closure temperatures [20]. It was also found that diffusion coefficients for trace elements in plagioclase decrease by up to four orders of magnitude (e.g., Sr) with increasing of anorthite content, and are smallest for anorthitic plagioclase [18,21]. This, in combination with the large size (2–25 mm) of these megacrysts, implies that the crystals were closed to exchange with the surrounding magma after their formation and preserve the trace element concentrations established during growth from the parental melts.

3. Occurrence and petrography of anorthite megacrysts in arc magmas

High-anorthite plagioclase occurs as large phenocrysts (or megacrysts) in high-alumina basalts throughout the Kurile Island Arc. In most cases the phenocryst assemblage includes euhedral olivine and olivine–anorthite cumulate inclusions. Similar anorthite megacrysts are also often found as relic phases in andesites, rhyolites and hybrid rocks in almost every studied volcanic center, both subaerial and submarine. In many cases, the anorthite megacrysts are present in association with olivine–anorthite and less frequently with olivine–anorthite–clinopyroxene and olivine–anorthite–amphibole cumulate inclusions, with clinopyroxene and amphibole occurring in interstices [4,22–26]. Where inclusions are found, the anorthite megacrysts frequently have an anhedral shape which results from breakage of the cumulate inclusions. Euhedral and anhedral megacrysts are chemically identical with anorthites in the associated inclusions [23,24]. $^{87}Sr/^{86}Sr$ ratios in megacrysts [24] and anorthite-rich inclusions [5] are identical to their host rocks suggesting that they represent the products of cognate crystallization of similar age. In addition, the presence of non-devitrified melt inclusions and fresh appearance suggest that most anorthite megacrysts studied are arc-related, and not xenocrysts in the sense that they came from the older pre-arc basement rocks. Even if they represent cumulates or protocrysts, their chemistry is defined by the host volcano which is linked to the Benioff zone depth. Therefore, no matter how complicated and multistage the history of each given megacryst was, its trace element concentration inherited from the initial primitive melt is preserved and can be used to monitor the chemistry of magma at each Benioff Zone depth.

Table 1 and Fig. 1 summarize megacryst occurrences studied here. Anorthite megacrysts are much more abundant in the Kuriles and Kamchatka than was previously thought (e.g., [22,23]). Twenty years ago they were considered to be a peculiar feature of certain volcanic centers, especially those belonging to the frontal low-K, high-alumina basalt zone [22]. Extensive dredging from the rear arc and more detailed investigations of subaerial rear-arc volcanics have shown that they are also present as rare large phenocrysts in high-K basalts.

Similar anorthite megacrysts have been found and described in other volcanic arcs — Japan [24], Vanuatu [15], Lesser Antilles [25] — and are commonly believed to be a feature of primitive arcs, formed largely on oceanic crust. However, because the number of such occurrences increases year by year and includes some continental arc localities such as Central Kamchatka [22], Central Japan [24] and Guatemala [27], the role of these megacrysts appears to be underestimated. Anorthitic plagioclase is also found in boninites [28], some alkali basalts [30], and are very common in MORB [29,31].

Textural observations in basalts and in olivine–

Table 1
Anorthite megacryst occurrences in the Kurile Island Arc

#	Sample	Volcano	Benioff Zone depth (km)	Rock types	Analyzed range of An (% in cores)	Maximal size (mm)
1	116b	Golovnin	115	rhyolitic pumice (72.00)	97–89	25
2	MR-1	Mendeleev	128	hybrid dacite (63.00)	92–82	10
3	Bar-3	Baransky	130	andesite (57.91)	90–88	5
4	B-540	Bogdan Khmelnitsky	160	basalt (51.15)	95–92	5
5	B-646	Kudriavy–Medvezhy	127	basaltic andesite (56.19)	91–89	5
6	*B25-24/3*	Volc. 7.11A	150	basaltic andesite (56.97)	93–90	2
7	*B15-81/1*	Volc. 7.10	163	basaltic andesite (53.41)	93–90	2
8	*B17-40/6*	Volc. 8.2	193	basaltic andesite (53.35)	88–86	2
9	*B17-41/4*	Volc. 8.11	203	basalt (51.60)	86–83	2
10	Zav-3	Zavaritsky	140	dacitic pumice	95–90	10
11	R135-1	Vetrovoi	168	andesite	92–91	3
12	92-223	Alaid	220	basalt	91–89	2

Numbers in italics are for dredged samples; An, %, proportion of anorthite; numbers in brackets are SiO_2 content of the host rock, where known.

anorthite inclusions indicate that anorthite crystals often enclose earlier $Fo_{82–76}$ olivine, although they are less commonly found in olivine as inclusions. It is interpreted that plagioclase is the first or second (after olivine) liquidus phase regardless of magma chemistry (e.g., [22,23]). Interstitial clinopyroxene is often found in inclusions, pointing to its crystallization after olivine and anorthite. Confirming that order of mineral appearance are gabbroic and troctolitic clinopyroxene–bytownite inclusions on some volcanoes (e.g., Chirinkotan, Bogdan Khmelnitsky), which represent a phenocryst paragenesis which is later than olivine–anorthite.

Melt inclusion studies in anorthite and olivine from several Kurile–Kamchatka volcanoes [32] and MORB [31] revealed that the composition of homogenized melt inclusions is high-Al basalt with ~4–7% of MgO, and T_{hom} in the range of 1050–1100ºC suggesting ~1.5–2 wt% H_2O.

4. Constraints on anorthite crystallization conditions

Phase equilibria studies have shown that plagioclase is an early liquidus phase in most arc magmas [16,17,33]. High Ca/(Ca + Na) ratio and water content of the melt are factors favorable for the crystallization of high-Ca plagioclase from basalts of varying chemistry and tectonic setting [16].

Among extensive experimental literature on basalt crystallization, recent numerical crystallization routines (e.g., MELTS and COMAGMAT) have the advantage of combining multiple experimental results covering the wide range of intensive and extensive parameters, and yield reasonable agreement with more specific physical experiments [34].

Numerical crystallization modeling using the MELTS program [35] was performed in order to reveal $P–T–X_{H_2O}$ conditions of anorthitic plagioclase crystallization by varying pressures and water content and composition within ranges of basic magmas (Fig. 2). Since, in nature and experiments, anorthitic plagioclase appears on the liquidus in melts with high CaO/Na_2O and Al_2O_3 content [16], we choose starting compositions to match high-alumina arc basalts of low-K tholeiite from the front arc and high-K basalt from the back arc (Table 2). These compositions match the compositions of melt inclusions in anorthite and olivine phenocrysts (e.g., [31,32]).

The temperature at which anorthitic plagioclase appeared on liquidus varied from 1200ºC at 0.5 wt% of H_2O down to 1050–1100º at 2.5–3.5 wt% of H_2O. By varying the composition of each oxide within the indicated values (see Table 2), we found that highly anorthitic plagioclase (An > 86%) only appears in basalts with high Ca/Na and Al_2O_3 (typically >19 wt%) and low Na_2O content (<2.5 wt%). Variation in CaO above 10 wt% has less effect. Significantly,

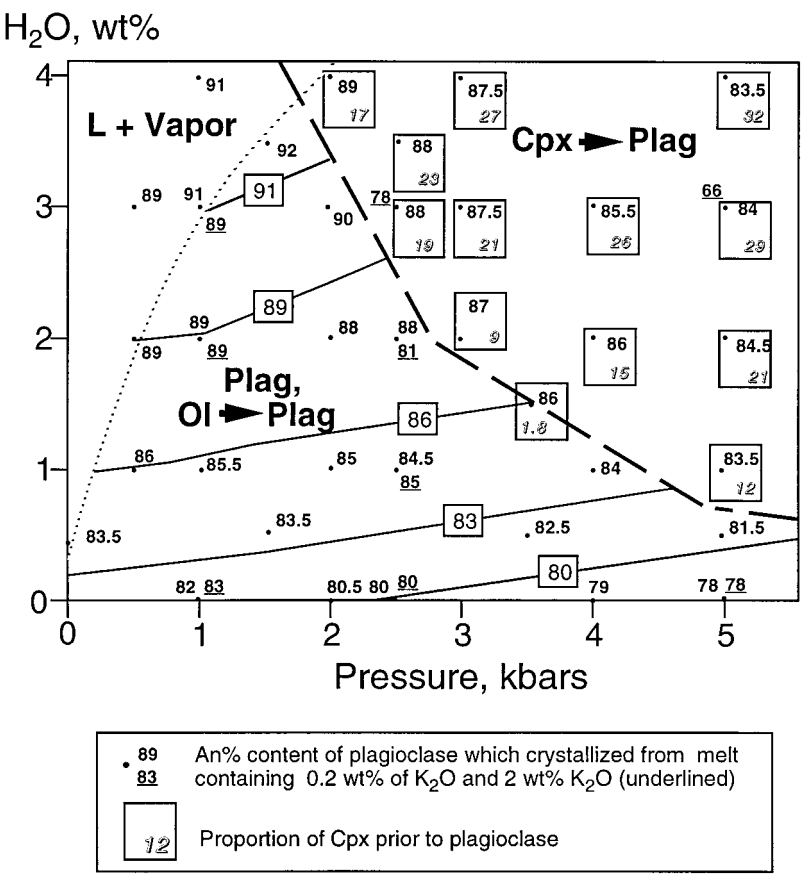

Fig. 2. The $P-X_{H_2O}$ diagram with isopleths of plagioclase composition constructed based on numerical crystallization experiments with compositions shown in Table 2. Dashed line represents a boundary where clinopyroxene crystallization occurs prior to plagioclase; dotted line represents water saturation.

Table 2
The starting compositions of melt, used in numerical crystallization experiments; values in brackets show ranges of concentrations with which numerical experiments were conducted

Oxide	wt%
SiO_2	48.96 (47–55)
TiO_2	0.81
Al_2O_3	19.90 (18–23)
Cr_2O_3	0.10
FeO*	10.00 (7–13)
MnO	0.10
MgO	8.00 (4–10)
CaO	10.00 (9–13)
Na_2O	2.01 (1–3)
K_2O	0.20 (0.1–2)
P_2O_5	0.10
Sum	100.17

we found that increasing K_2O contents up to 2 wt% (to cover the range of Kurile's across-arc variations) produces little effect on the An content of the crystallizing plagioclase (see Fig. 2). However, it increases the proportion of clinopyroxene relative to olivine at higher pressure, thus prematurely depleting the melt and plagioclase in Ca. Decrease in MgO (from 10 to 4 wt%) or increase in FeO* produces almost no direct effect on plagioclase composition. It slightly decreases the proportion of clinopyroxene relative to olivine prior to plagioclase at higher pressures (2.5–5 kbar), thus slightly increases An% of plagioclase by 1–2 mol%. Similarly, an increase in oxygen fugacity from IW to HM buffers only slightly decreases An% by 3 mol%. This implies that under conditions when major clinopyroxene crystallization has not occurred prior to plagioclase crystallization,

neither K_2O content of the magma nor MgO and Mg# are capable of significantly changing the anorthite content of plagioclase. This is in an agreement with the above observations that similar anorthite is found throughout the arc regardless of host magma K_2O content.

Increased H_2O content strongly favors crystallization of An-richer plagioclase: an increase from 0.5 to 3 wt% under fixed conditions leads to 10 mol% increase in An%. Increase in lithostatic pressure is less effective and acts in the opposite direction, in agreement with experiments [16,33]. However, pressure causes a marked decrease in An% of plagioclase in an indirect way. Clinopyroxene becomes an increasingly dominant liquidus phase appearing before plagioclase at pressures higher than 2.5 kbar, and thereby reducing the CaO/Na_2O of the melt and An% of plagioclase (Fig. 2). Crystallization of highly calcic plagioclase with An > 90% only occurs when it appears before clinopyroxene.

Our modeling indicates that even if the MgO of the original basic magma was in the typical 7–9 wt% range, then under the described conditions 1–10 wt% of magnesium olivine fractionation prior to plagioclase is capable of reducing the MgO melt content to 3–5 wt%. As a result, the first highly-anorthitic plagioclase coexists with chrisolitic olivine (Fo_{75}) in accordance with observations [22,23].

The optimal condition for crystallization of high-An plagioclase includes pressures less than 2.5 kbar and 1.5–3 wt% of water; this ensures no significant clinopyroxene crystallization prior to plagioclase. It indicates that crystallization occurs at 3–8 km depth, corresponding to magma chambers under Kurile Arc volcanoes [13]. These rather shallow and water-rich conditions of crystallization are reflected in the highly vesicular appearance of olivine–anorthite inclusions in the Kurile–Kamchatka Island Arc and the often explosive character of their eruption [26].

Therefore, when highly anorthitic plagioclase is found, it implies that no significant clinopyroxene crystallization has occurred prior to anorthite. Clinopyroxene is the only likely liquidus mineral which has non-negligible partition coefficients for many trace elements, such as HREE. We found that plagioclase persists as a liquidus phase in most high-Al basalts, though olivine, spinel and orthopyroxenes may crystallize before plagioclase at high water pressures regardless of the K_2O content of the melt. Early fractionation of these phases (even with some clinopyroxene) prior to plagioclase is capable of significantly changing only MgO, Mg/Fe ratio and ferromagnesian (siderophile) trace element concentrations (e.g., Ni, Co, V, Cr), elements which are strongly compatible with the earliest cumulates. All other trace elements are incompatible with this early cumulate assemblage and can only suffer insignificant (10–20%) proportional increase in the residual melt.

5. Procedure and analytical technique

Thin sections with anorthite megacrysts (see Table 1) were first studied under the microscope and then with secondary and back-scattered electron imaging on a JEOL JSM-5800LV scanning electron microscope (SEM) at the University of Chicago. Wavelength-dispersive analyses for major elements were made on a Cameca SX-50 electron microprobe using a standard procedure (15 kV, 10 nA, 2–5 μm). Synthetic and natural minerals were used as standards. Samples which were imaged with the SEM and analyzed by electron microprobe were analyzed later at the same spot by ion microprobe. Ion microprobe analyses were made using a modified AEI IM-20 instrument at the University of Chicago for concentrations of: Li, Be, B, F, Mg, P, Cl, K, Ti, Fe, Co, Rb, Sr, Y, Zr, Nb, Cs, Ba, La, Ce, Pr, Nd, Sm, Eu, and Pb. Trace element-bearing NBS glasses were analyzed as standards at the beginning and end of each day of analyses to correct for 5–10% in ion yield variations. The analytical techniques used here are similar to those described in [36,37]. Molecular interferences were reduced by energy-filtering. For each sample, six cycles through the mass peaks were made. The sputtering history of each spot was checked for any increase in concentrations of trace elements resulting from glass or mineral inclusion contamination. Clearly discrepant analyses were rejected. We normally analyzed at least two spots in each plagioclase core. Whole-rock trace element and isotope analyses were made in the laboratories of the Geologisk Institut, University of Copenhagen (see [4,12] for analytical details).

6. Compositional profiles through megacrysts

We performed electron microprobe profiles through selected megacrysts from each volcano (Table 1), and found a pronounced homogeneity of anorthite megacryst cores with respect to major elements, normally within 2 mol% of anorthite content, as was noted earlier (e.g., [22,23]).

Trace element profiles through a number of representative An-rich crystals in hybrid dacite of Mendeleev Volcano (Kunashir Island) were established to test whether a 'plateau value' on concentration of trace element–distance plot is preserved even for a phenocryst resided within hybrid silicic magma. Magma mixing between rhyolitic and basaltic andesitic magmas is demonstrated for the host dacite [38]. Similar An_{84} calcic plagioclase megacrysts with 0.01 wt% of K_2O are found in basaltic andesites, while plagioclase in rhyolite is $An_{40–45}$ with 0.09 wt% of K_2O. Both basaltic andesites, rhyolite, and hybrid dacite have the same $^{87}Sr/^{86}Sr$. The origin of rhyolite is most consistent with 50–65% fractionation of basaltic andesite magma. Both progressive enrichment of the melt with K_2O due to fractionation (factor of 3–4) *and* increase in D_K with decreasing An-content from An_{84} to An_{50} (factor of 2–2.5) [38], are responsible for ~8+ increase in K_2O concentration (and other similarly incompatible trace elements) in phenocryst rims (Fig. 3).

Most trace elements were found to exhibit a plateau-type profile, except for some small ions — Li, Be, as well as halogens — with more irregular patterns. This is taken to indicate that the unzoned cores have retained most of their trace elements (Fig. 3), despite a magma mixing episode resulting in a strong core–rim concentration gradient. Phenocrysts from other volcanoes which had not experienced such a complicated history, are expected to preserve the original trace element concentrations within their 'plateau' cores.

7. Across-arc variations of trace element concentrations in anorthite megacrysts

Given the narrow compositional range of plagioclase megacrysts (An_{84}–An_{94}), the across-arc chemical variations can be displayed by direct comparison of trace element concentrations in megacrysts with depth to the Benioff Zone (Table 3, Fig. 4). The concentrations of minor and trace elements in plagioclase that can be measured with good accuracy, such as K, Sr, Ba, La, Ce and several other key trace elements, all exhibit clear linear variations with depth to the Benioff Zone. Elements whose concentration in the whole rock (and correspondingly plagioclase) is low (e.g., Pr, Nd, Sm, Cs) and/or low in plagioclase due to small plagioclase/melt partition coefficients (e.g., Cs, Rb, Zr, Nb), exhibit larger scatter which may also include some natural diversity.

Levels of Fe, Mg, and therefore Mg/Fe remain approximately constant across the arc though with significant scatter. Concentration of Co, the only other measured fractionation-sensitive trace element, also lacks any trend across the arc. This suggests that there is no variation in the degree of fractionation across the arc prior to the appearance of anorthite on the liquidus. Since Mg and Fe^{2+} were shown to have similar plagioclase–melt partition coefficients [39], the Mg/Fe^{2+} ratio in plagioclase should directly reflect that of the parental magma. The low Mg/Fe ratio in Kurile and other natural plagioclases (compared to expected high Mg/Fe^{2+} ratio in primitive mantle-equilibrated basalts) is likely to reflect the fact that a significant proportion of iron in plagioclase is represented by ferric iron, which tends to partition into plagioclase ten times more efficiently than ferrous iron [39].

A least-square approximation routine [40] was used to determine the magnitude of linear increase or decrease of trace element variations in anorthite megacrysts across the arc (Fig. 5). This routine weighs each sample as a function of its error bars. In addition, outliers which are beyond 2σ of the approximation line, and are shown in italics in Table 2, are excluded. Fig. 5 shows the calculated maximum trace element enrichment or depletion factor in the rear arc relative to the volcanic front, represented as trace element ratio normalized to depths of 220 km (rear arc) versus 120 km (volcanic front), as taken from the approximation line. The magnitude of this ratio should adequately reflect the ratio for parental melts, since plagioclase has virtually constant anorthite content across the arc, and accordingly plagioclase–melt partitioning is expected to be the same [37].

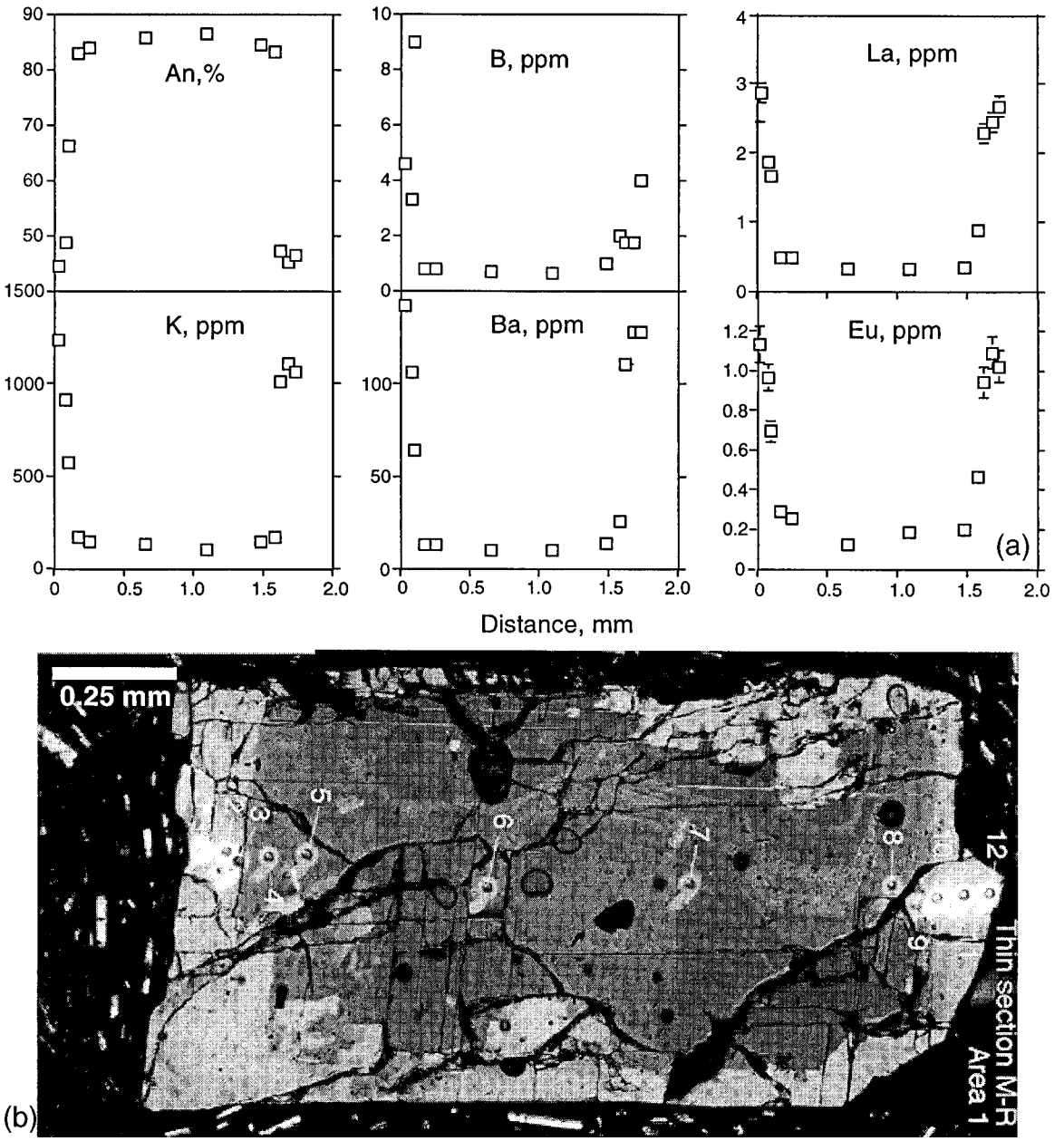

Fig. 3. (a) Chemical profiles through a relic Ca-rich plagioclase megacryst in dacite of Mendeleev Volcano (Kunashir Island). Notice that a 'plateau' is preserved for several trace elements. (b) Micrograph through the indicated megacryst; dark Ca-rich core is clearly preserved, whereas light rim areas are Ca-poor overgrowths as a result of residence in the dacitic magma. Phenocrysts in the dacite have similar rim compositions.

We find that the concentrations of Ba and K in megacrysts show the maximum increase across the arc by a factor of 12, similar to but larger than that displayed by the whole-rock data (see Fig. 6 below and [3,5,6]). Smaller increases are exhibited by other lithophiles: Li, Sr, and Be. Variations in Rb and especially Cs are less certain due to the low abundance in plagioclase, and may even follow

Table 3
Averaged trace element concentrations in anorthite megacrysts from studied volcanic centers of the Kurile Island Arc

Sample	116B	B-646	MR-10	BAR-3	Zav-3	B25-24/3	B540	B15-81/1	R135-1	B17-40/6	B17-41/4	92-223
Volcano	Golovnin	Kudriavy	Mendeleev	Baransky	Zavaritsky	Volc. 7.11A	Bogdan Khm.	Volc. 7.10	Vetrovoi	Volc. 8.2	Volc. 8.11	Alaid
H (km)	115	127	128	130	140	150	160	163	168	193	203	220
n	5	3	5	2	2	2	4	3	4	4	3	4
An (%)	94.5 ± 0.4	92.5 ± 0.1	84.8 ± 0.6	94.5 ± 0.6	88.8 ± 2.1	92.2 ± 0.6	91.7 ± 1.3	90.9 ± 1.4	92.1 ± 0.1	85.9 ± 0.3	84.4 ± 0.9	89.0 ± 0.4
Trace element concentrations (ppm)												
Li	0.36 ± 0.03	0.97 ± 0.20	*16.62 ± 0.54*	0.25 ± 0.02	0.14	0.40 ± 0.03	0.28 ± 0.09	0.55 ± 0.12	0.23 ± 0.04	0.60 ± 0.01	0.78 ± 0.07	*0.01*
Be	0.06	0.11 ± 0.01	*1.46 ± 0.05*	0.07 ± 0.01	0.11	0.14 ± 0.03	0.08 ± 0.01	0.12	0.09	0.16 ± 0.01	0.08	0.15 ±
B	0.14 ± 0.01	0.29 ± 0.03	*1.29 ± 0.54*	0.35 ± 0.01	0.18	0.10	0.22 ± 0.04	0.21 ± 0.04	0.28 ± 0.01	0.15 ± 0.01	0.17 ± 0.01	0.13 ± 0.01
F	9.1 ± 6.7	20.3 ± 5.8	15.8 ± 1.0	37.5 ± 0.6	43.5	9.0 ± 1.5	27.5 ± 3.2	4.3 ± 2.2	19.8 ± 1.3	28.0 ± 2.8	38.O ± 4.5	22.3 ± 4.1
Mg	456 ± 124	416 ± 14	*127 ± 10*	307 ± 24	364	238 ± 10	364 ± 101	340 ± 30	323 ± 4	365 ± 14	486 ± 190	345 ± 15
P	18 ± 6	30 ± 1	30	18 ± 2	14 ± 3	21 ± 5	27 ± 3	21	51 ± 2	65 ± 3	63 ± 5	49 ± 5
Cl	50 ± 6	57 ± 8	47 ± 3	89 ± 21	47 ± 2	44 ± 2	67 ± 3	86 ± 9	77 ± 3	60 ± 5	56 ± 2	62 ± 6
K	33 ± 33	74 ± 6	140 ± 14	142 ± 11	128 ± 3	153 ± 15	329 ± 67	279 ± 47	226 ± 3	381 ± 29	664 ± 233	519 ± 30
Ti	55 ± 24	55 ± 2	81	65 ± 1	58	53	94 ± 12	84 ± 9	73 ± 1	124 ± 9	188 ± 38	107 ± 4
Fe	3550 ± 296	3820 ± 42	2827 ± 224	3790 ± 53	2853 ± 204	3326 ± 101	2566 ± 181	3049 ± 109	3677 ± 96	3448 ± 87	2868 ± 660	3555 ± 46
Co	2.90 ± 0.43	5.10 ± 0.70	2.96 ± 1.30	6.40 ± 0.49	6.40 ± 0.81	6.90 ± 1.15	2.93 ± 0.64	4.40 ± 2.50	3.38 ± 0.65	6.43 ± 0.58	3.93 ± 0.86	4.03 ± 1.23
Rb	0.24 ± 0.11	0.30 ± 0.04	0.27	0.70 ± 0.06	<0.16	0.81 ± 0.19	0.75 ± 0.43	0.37 ± 0.04	0.18 ± 0.03	0.43 ± 0.11	*3.84 ± 1.22*	0.42 ± 0.08
Sr	269 ± 10	432 ± 1	447 ± 6	359 ± 29	774	714 ± 40	762 ± 45	621 ± 1	917 ± 1	1234 ± 18	1367 ± 69	1312 ± 14
Y	0.10 ± 0.07	0.16 ± 0.01	0.36 ± 0.07	0.75 ± 0.01	0.49	0.21 ± 0.01	0.32 ± 0.12	0.18 ± 0.01	0.23	0.34 ± 0.02	0.33 ± 0.01	0.29 ± 0.02
Zr	0.07 ± 0.02	0.12 ± 0.02	0.08 ± 0.01	0.15 ± 0.01	0.45 ± 0.02	0.20 ± 0.10	0.16 ± 0.05	0.23 ± 0.03	0.13 ± 0.01	0.28 ± 0.10	0.09 ± 0.02	0.20 ± 0.03
Nb	0.05 ± 0.01	0.02 ± 0.01	0.01 ± 0.00	0.05 ± 0.01	0.04	0.02	0.08 ± 0.02	0.06 ± 0.02	0.04 ± 0.01	0.04 ± 0.01	0.13 ± 0.06	0.03 ± 0.01
Cs	0.05 ± 0.01	0.06 ± 0.02	<0.02	0.06 ± 0.01	<0.01	0.05 ± 0.03	<0.03	<0.03	<0.01	0.04 ± 0.01	*0.20 ± 0.07*	0.12 ± 0.02
Ba	3.8 ± 1.0	5.7 ± 0.1	14.5 ± 1.1	10.5 ± 1.2	11.0 ± 0.3	21.0 ± 3.0	17.1 ± 4.4	18.7 ± 0.3	18.5 ± 0.1	39.5 ± 1.2	53.0 ± 4.0	50.5 ± 1.2
La	0.61 ± 0.06	1.00 ± 0.25	0.46	0.90 ± 0.07	1.00	1.00	0.64 ± 0.17	0.67	0.88 ± 0.07	1.25	2.67 ± 0.17	*6.00 ± 0.25*
Ce	1.08 ± 0.06	1.93 ± 1.11	1.03 ± 0.06	2.00 ± 0.10	1.50 ± 0.04	1.10 ± 0.15	1.20 ± 0.62	1.23 ± 0.06	1.63 ± 0.16	2.45 ± 0.03	4.80 ± 0.51	*15.87 ± 1.11*
Pr	0.12 ± 0.01	0.17 ± 0.03	0.15 ± 0.01	0.28 ± 0.01	0.12 ± 0.01	0.15 ± 0.02	0.14 ± 0.06	0.13 ± 0.01	0.15 ± 0.01	0.26 ± 0.01	0.54 ± 0.09	0.59 ± 0.03
Nd	0.33 ± 0.06	0.61 ± 0.01	0.58 ± 0.03	1.10 ± 0.03	1.42 ± 0.03	0.78 ± 0.15	0.64 ± 0.18	0.56 ± 0.03	0.65 ± 0.02	0.97 ± 0.02	1.73 ± 0.13	1.28 ± 0.01
Sm	0.17 ± 0.02	0.10 ± 0.03	0.10 ± 0.01	0.23 ± 0.01	*1.03 ± 0.03*	0.18 ± 0.01	0.18 ± 0.04	0.12 ± 0.02	0.16 ± 0.02	0.19 ± 0.02	0.24	0.27 ± 0.03
Eu	0.11 ± 0.01	0.08 ± 0.02	0.25	0.15 ± 0.01	0.04 ± 0.01	0.20 ± 0.02	0.18 ± 0.04	0.22 ± 0.02	0.16 ± 0.01	0.32 ± 0.01	0.60 ± 0.04	0.31 ± 0.02
Pb	2.15 ± 1.22	2.33 ± 0.13	2.60 ± 0.30	15.00 ± 0.43	7.50 ± 0.75	4.50 ± 1.25	13.60 ± 0.86	6.00 ± 0.77	3.50 ± 0.22	7.25 ± 0.53	4.67 ± 1.45	2.25 ± 0.13

See Table 1 for sample description. ±1σ values are given only when they are larger than 5% of the value. Numbers in italics are outliers beyond 2σ on Fig. 4 approximation line.

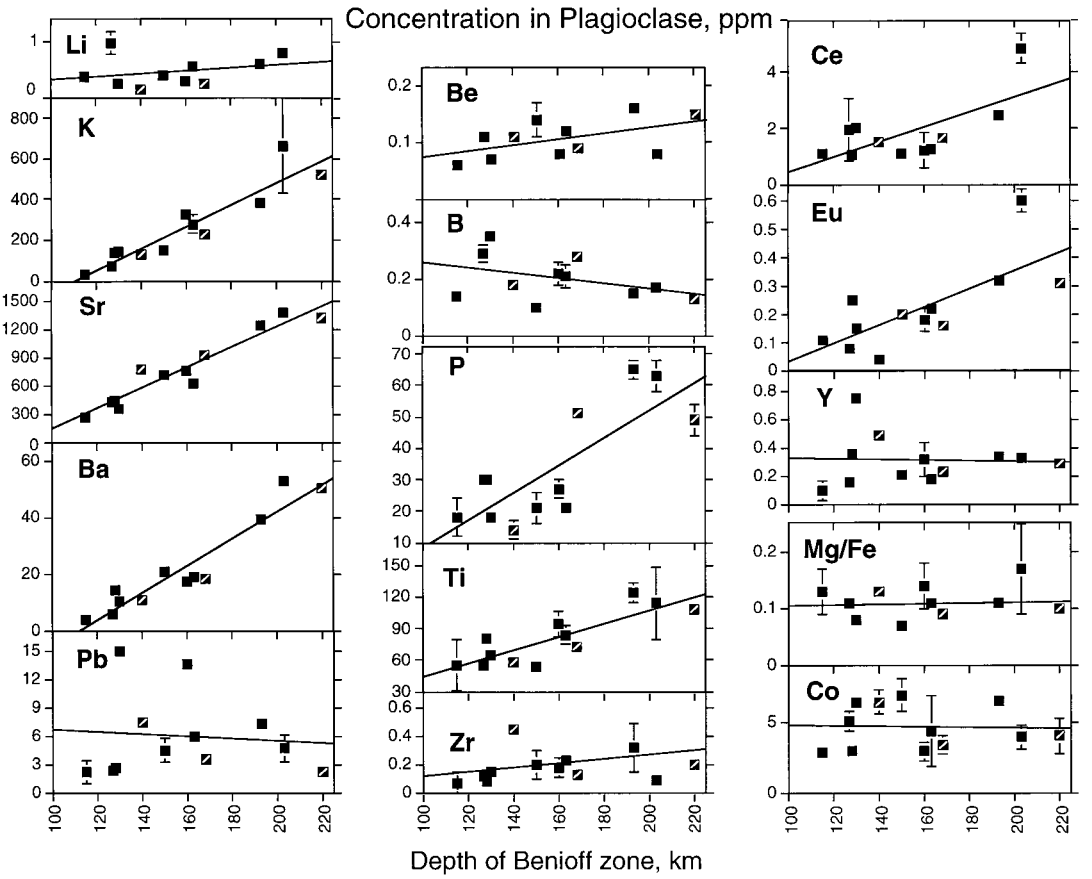

Fig. 4. Ion microprobe-measured trace element concentrations in anorthite megacrysts as a function of Benioff Zone depth. Data from Table 2. Each point represents the averaged concentration for a volcanic center; error bars are $\pm 1\sigma$ of averages of trace element concentrations in several anorthite megacryst cores. Symbols with a slash inside denote northern and central Kuriles, the rest is from southern Kuriles; note that no along-arc variations are seen.

the decreasing trend (see Fig. 4) for hydrophile elements.

Eu and light REE show an increasing enrichment toward the rear arc. Remarkably, the enrichment factor for REE decreases steadily along with ionic radius from La to Sm. Heavier REE, Sm and the heavy REE-element proxy Y show no enrichment. Eu, on the other hand, deviates from this general rule and shows the strongest enrichment. Since a significant proportion of Eu is likely to be present in Eu^{2+} form over the range of oxygen fugacities in Kurile magmas [10,41], the charge and size of Eu^{2+} make it behave as an element analogue of Sr [42], allowing it to follow the same line of behavior across the arc like Sr^{2+}.

Measured HFSE also exhibit a slight increase in concentration toward the rear arc, or remain constant. Hydrophile elements — Cl, F, Pb and B — show significant scatter and either remain constant or decrease with deepening of the Benioff Zone.

The established pattern of enrichment is generally consistent with the whole-rock across-arc trends for LILE, LREE, HFSE, and volatile, hydrophile elements [3,6,43]. In particular, the decrease in B, Pb and increase in Be are consistent with the data of [44,45] and [9,43]. However, as pointed out above, the linear approximation, especially for trace elements with dual affinities to melts and fluids (e.g., Cs, Rb, Pb), may not reflect the full range of processes across the arc.

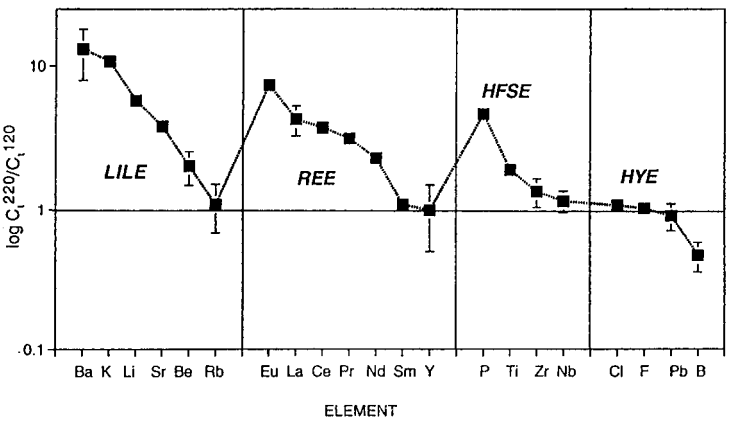

Fig. 5. Ratio of best-fitted trace element concentrations at the depth of 220 km (rear arc) over 120 km (volcanic front), showing the maximal possible magnitude of trace element enrichment/depletion factors across the arc. Elements are arranged in decreasing order in four groups: lithophile (*LILE*), rare earths (*REE*), high field-strength (*HFSE*), and hydrophile (*HYE*) elements. Note the sequence of trace element enrichment/depletion.

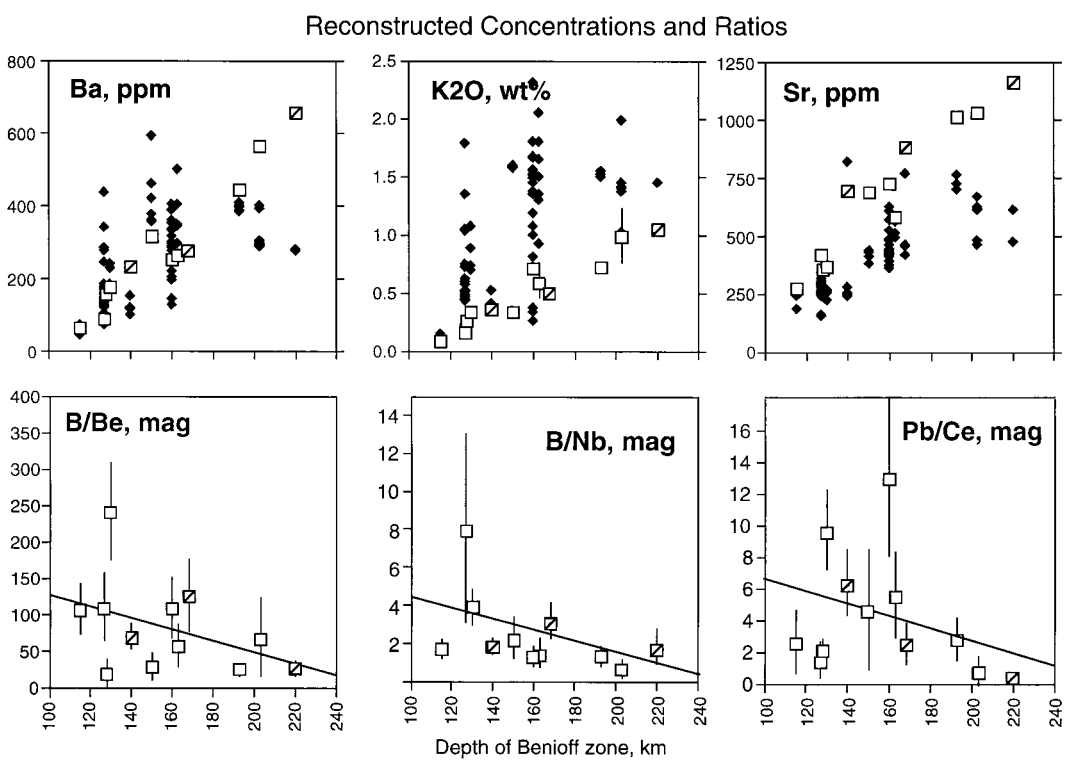

Fig. 6. Reconstructed concentrations and ratios of trace elements in parental magmas of anorthite megacrysts (large empty squares) as compared with measured whole-rock trace element concentrations for the most primitive mafic volcanics (basalts and basaltic andesites) found at these centers (filled diamonds); whole-rock data are from [5] and Bindeman and Bailey (unpublished data). Note that the reconstructed concentrations for most incompatible trace elements are systematically lower, and for the compatible element Sr are higher, than concentration in the whole-rock. This is taken as evidence that anorthite megacrysts tap a more primitive (less differentiated) stage than is represented by the whole-rock (see text for discussion and Fig. 4 for symbol explanation).

8. Reconstructed concentration of trace elements in parental magmas versus whole-rock concentrations

Dividing the measured concentrations of trace elements in plagioclase by the appropriate partition coefficient allows the reconstruction of trace element concentrations in parental melts (Fig. 6). However, only elements which are abundant in plagioclase (K, Li, Mg, Sr, Ba, LREE) and for which partition coefficients are non-negligible can be used successfully. We used ion microprobe-based plagioclase–basalt partition coefficients [37], which were determined using the same University of Chicago ion microprobe, using the same procedure and the same list of trace elements. All trace element partition coefficients show a linear relationship of the form: $RT\ln(D_i) = aX_{An} + b$, which allows correction to D_i's depending on plagioclase composition. The expected ~50–100ºC range between temperatures of plagioclase crystallization in Kurile Arc basalts of different alkalinity and water content is a less important factor than plagioclase composition, and contributes less than 5% to the $RT\ln(D_i)$ parameter [37]. We took ~1200ºC and 1150ºC as liquidus temperatures for front-arc tholeiitic and rear-arc high-K basalts, respectively, based on their plagioclase crystallization temperatures calculated in MELTS program [35] above.

We found (see Fig. 6) that for most incompatible elements the reconstructed concentrations are ~70–100% of those in the whole rocks containing these phenocrysts. For Sr we observed the opposite situation. Sr readily enters plagioclase ($D^{Pl}_{Sr} > 1$) and is likely to be compatible with the earlier plagioclase-dominated cumulate assemblage during basalt fractionation. The most undifferentiated basalts found at some volcanoes often overlap with the reconstructed primitive values. However, not all volcanoes have such basalts present at the surface. The result is that reconstructed compositions are collinear (comagmatic) with the whole-rock data but give systematically less differentiated compositions for several key trace elements. This does not appear to be an artifact of the partition coefficient model. Rather it implies that anorthite megacrysts tap a more primitive stage of basalt segregation than that represented by the whole-rock data. It emphasizes that the anorthite megacrysts are the result of crystallization from a more primitive magma than the host rock.

The reconstructed MgO concentrations based on the studied anorthite crystals are 3–5 wt%, typical for high-Al basalts which have only suffered olivine and spinel fractionation (e.g., [1]). Interestingly, the measured MgO concentrations in melt inclusions inside coexisting anorthite and olivine from four Kurile and Kamchatka volcanoes (e.g., [32]) are also in the 3–7-wt% range. The MELTS modeling presented above shows that the decrease in MgO content and Mg/Fe ratio in the melt produces a weak direct influence on plagioclase composition.

More information on the trace element budget across the arc is provided by trace element ratios of different geochemical groups (e.g., Fig. 4). In particular, ratios of hydrophile elements to HFSE usefully constrain the role of fluids in magma genesis, since HFSE do not participate in dehydration reactions [44–46], and serve as a good reference element group for hydromagmatic element normalization. B/Be and B/Nb ratios reconstructed from anorthite megacrysts, and from whole-rock values [6,9,42–44], decrease across the arc. There is also a decreasing trend in Pb/Ce ratios, confirming the hydrophile nature of Pb in arc magmas. We also see an increasing trend in LILE/HFSE ratios (e.g., K/Nb, Ba/Zr) across the arc which is not resolved in whole-rock analyses [9].

9. Isotope ratios

Newly determined isotope ratios of $^{87}Sr/^{86}Sr$, $^{143}Nd/^{144}Nd$, $^{206}Pb/^{204}Pb$, $^{207}Pb/^{204}Pb$, $^{208}Pb/^{204}Pb$ for primitive samples found on volcanoes (some of them with highly anorthitic plagioclase) are given in Table 4 and plotted on Fig. 7, along with the published isotope ratios for the same volcanoes. Studied samples plot in the middle of the reported trend for strontium and neodymium isotopes and confirm the across-arc trend, previously established for the Kuriles [7,8]: a decrease in both $^{87}Sr/^{86}Sr$ and $^{143}Nd/^{144}Nd$. Results for lead isotopes across the Kuriles show the absence of any trend in Pb isotope ratios. All Pb isotopes lie just within the reported MORB values for the northern Pacific (see Fig. 7), and require little or no sediment or fluid addition.

Table 4
Whole-rock isotope composition of primitive basic rocks from Kurile Island Arc

Sample	Volcano	Benioff Zone depth (km)	Rock type	$^{87}Sr/^{86}Sr$	$^{143}Nd/^{144}Nd$	ε_{Nd}	$^{206}Pb/^{204}Pb$	$^{207}Pb/^{204}Pb$	$^{208}Pb/^{204}Pb$	Pb (ppm)
B552	Kudriavy	127	B (52.49)	0.703224	0.513100	9.01	18.381	15.494	38.152	5.8
B559	Kudriavy	127	BA (56.67)	0.703221	0.513105	9.11	18.385	15.514	38.234	7.0
B620	Kudriavy	127	BA (55.66)	0.703229	0.513115	9.30	18.376	15.510	38.213	4.7
B622	Kudriavy	127	A (57.71)	0.703233	0.513100	9.01	18.346	15.511	38.179	7.6
B631	Kudriavy	127	B (50.67)	0.703275	0.513106	9.13	18.353	15.510	38.194	2.9
B634	Kudriavy	127	B (50.5)	0.703259	0.513105	9.11	18.773	15.385	37.653	4.0
B652	Kudriavy	127	BA (53.55)	0.703196	0.513101	9.03	18.404	15.545	37.306	5.3
B657	Kudriavy	127	BA (53.34)	0.703194	0.513111	9.23	18.352	15.529	38.240	11.0
B357	Baransky	130	BA (54.81)	0.703189	0.513070	8.43	18.266	15.541	38.142	4.9
B25-24/7	Volc. 7.11A	150	A (58.48)	0.703159	0.513003	7.12	18.402	15.515	38.281	6.7
B540	Bogdan Khm.	160	B (51.15)	0.702881	0.513047	7.98	18.352	15.502	38.153	3.1
B541	Bogdan Khm.	160	B (50.87)	0.702911	0.513066	8.35	18.198	15.519	38.066	4.1
BIN-111	Bogdan Khm.	160	B (51.75)	0.702978	0.513048	8.00	18.329	15.515	38.182	5.3
BIN-112	Bogdan Khm.	160	B (49.99)	0.702952	0.513054	8.11	18.342	15.544	38.263	4.8
B539	Bogdan Khm.	160	A (55.19)	0.703181	0.513010	7.26	18.394	15.509	38.242	6.8
B15-81/3	Volc. 7.1	162	B (53.41)	0.702828	0.513018	7.41	18.424	15.528	38.303	6.7
B17-42/6	Volc. 7.16	189	B (51.43)	0.702956	0.513021	7.47	18.401	15.506	38.235	5.2
B17-40/1	Volc. 8.2	193	B (53.01)	0.702809	0.513032	7.69	18.485	15.512	38.258	5.5
B17-41/3	Volc. 8.1	203	B (51.54)	0.702832	0.513019	7.43	18.415	15.500	38.207	3.8
B17-41/6	Volc. 8.11	203	B (51.25)	0.702761	0.513021	7.47	18.419	15.509	38.235	4.1

Numbers in italics are for dredged samples; B, basalt; BA, basaltic andesite; A, andesite.

10. Discussion

Primitive, high-MgO–Ni–Cr (MgO > 10 wt%) basalts are only rarely found in Kurile volcanoes or in other island arcs. Picrites with MgO in excess of 16 wt% have been considered as the most primitive type of basalt [15,17], but these have not yet been found in the Kuriles. Some of the most primitive volcanics in the Kuriles occur on Alaid; they are high MgO–Ni–Cr basalts and could be in equilibrium with a mantle source; some of them are nepheline-normative [4]. In Vanuatu Island Arc, such rocks exhibit considerable heterogeneity, and up to three distinct trace elemental magma types can be found on one island [15]. The heterogeneity of the most primitive arc magmas may indicate that they came from small melt batches in the mantle wedge, batches which differed in composition/differentiation histories.

In the Kurile Island Arc, the presence of similar anorthite megacrysts (similar large sizes, morphology, composition and Mg/Fe ratio) in rocks of different alkalinity and incompatible trace element contents is a characteristic feature of high-Al basalts from volcanoes located at different elevations above the seismofocal zone. Their potentially widespread presence reflects the broadly similar major element compositions of the main basaltic magma types in the Kuriles, with the exception of K_2O which ranges up to ~1.6 wt% [4–7]. Variations in K_2O and in cumulative amounts of LIL and hydrophile trace elements do not seem to affect phase equilibria (see Fig. 2).

Given this background, we propose a 'high-Al stage' of basalt differentiation which is reflected in anorthite megacrysts. The euhedral and homogeneous anorthite megacrysts are likely to form in large, slowly cooling magma chambers. The 'high-Al stage' represents a 'homogeneous' stage of mafic magma fractionation which is common for magmas across the arc. The results of MELTS modeling above and crystallization experiments indicate that anorthite crystallizes from relatively low pressure and hydrous magmas, not more than 10–15% after early olivine + spinel fractionation. Crystallization can proceed in the rather shallow and large

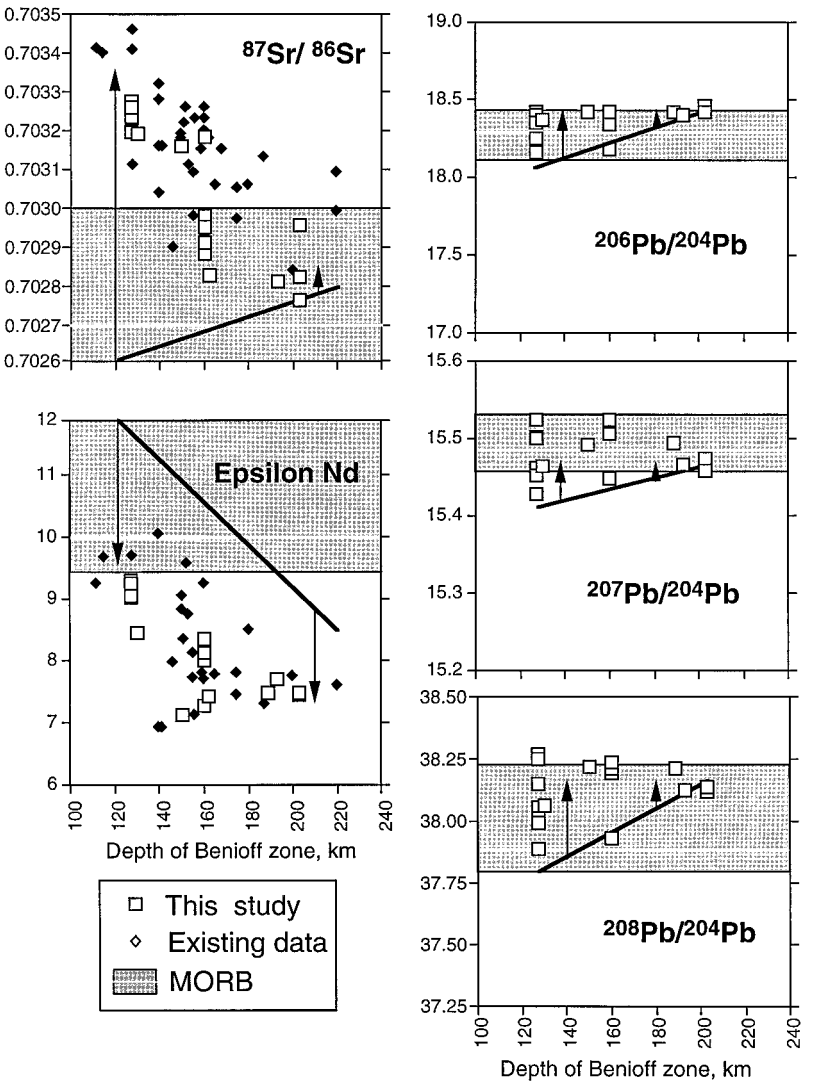

Fig. 7. Isotopic variations in rocks across the Kurile island arc from this study (large empty squares). Other published ratios are smaller filled diamonds, data from [7,8]. Grey fields with horizontal lines are ranges and averages of MORB values for Pacific [44,47,48]. Lines indicate assumed location of mantle sources before variable addition of slab-derived fluids (arrows), based on [7,8,12]. See text for discussion.

crustal magma chambers at 3–8 km depth which are known under most of the Kurile's volcanoes from geophysical data [11]. These chambers are likely to be drainage pools and traps for smaller, deeper and more primitive and heterogeneous basaltic melts, and may thus average out their differences. Basaltic andesites, the most abundant rock type on the Kuriles (and other island arcs) [1] are residual magmas left after fractionation of these more primitive, high-Al basalts. Glass of basaltic andesitic composition often occurs interstitially in olivine–anorthite and gabbro–anorthositic cumulate inclusions [23,26].

On this basis, the use of plagioclase megacrysts and other early liquidus phases may be a convenient way of comparing magmas *at the same stage* of their evolution and of understanding more precisely the magnitude of across-arc chemical variations. The use of cores of relic plagioclase megacrysts allows

one to see back through the effects of fractional crystallization, mixing and secondary alteration to the more primitive, high-Al basaltic compositions which may not otherwise be present. Plagioclase serves as a stable host for these trace elements, and the alteration processes affecting many volcanic rocks on the surface or under water do not seem to affect contents in the cores of plagioclase megacrysts. The use of plagioclase megacrysts, however, is limited to elements which can be measured with high precision on the ion microprobe

The results of this study reveal the linear increase or decrease of trace element concentrations and ratios across the Kurile Island Arc (e.g., Figs. 4 and 6). Trends are especially clear for several incompatible trace elements whose concentrations are measured with high precision. The sequence and magnitude of trace element enrichments (Ba > K > Sr > LREE, see Fig. 5) are similar to experimental results involving fluids [49–51], and confirm the role of fluid-release as an important transfer mechanism for trace elements at different depths as subduction proceeds. This is especially supported by the across-arc variations of Be, B, and Pb concentrations and B/Be, B/Nb, and Pb/Ce ratios [4,9,43–45], since the distribution of B and Pb is dominantly controlled by fluid addition [46]. and for which plagioclase/melt partition coefficients are non-negligible.

The discovered linearity of many trends, as opposed to hyperbolic (Rayleigh-type) increase or decrease, expected as a result of a single process of devolatilization or partial melting, deserves special comments. Linearity is likely to prove critical for modeling across-arc processes. Linearity is likely to reflect a combination of two or more petrogenetic factors: variations in fluid release and the decrease in the degree of partial melting with depth, change of the melting source [47]. Across the Kuriles, falling $^{143}Nd/^{144}Nd$ and Zr/Nb ratios but rising contents of HFSE indicate a steady transition to less depleted mantle sources towards the rear arc [7,8]. At the same time, linear increase in K and related incompatible trace elements, and the inferred water content [10] which is believed to behave as an incompatible component during crystallization, can be linked to the decrease in magma volumes, and imply a steady fall in the percentage of melt remaining.

Further insight is provided by across-arc isotopic variations (Fig. 7). $^{87}Sr/^{86}Sr$ does not correlate positively with Pb isotopic ratios and negatively with $^{143}Nd/^{144}Nd$, as seen in NE Japan [48], and is taken as the evidence of sediment-derived fluid addition. In the Kuriles, $^{87}Sr/^{86}Sr$ correlates positively with $^{143}Nd/^{144}Nd$ [7] and no clear correlation is seen on Sr–Pb and Nd–Pb isotopic plots, since Pb isotopes are homogeneous and MORB-like across the arc. Compared to NE Japan [47], the high $^{143}Nd/^{144}Nd$ ratios and low $^{87}Sr/^{86}Sr$, $^{206}Pb/^{204}Pb$, $^{207}Pb/^{204}Pb$, and $^{208}Pb/^{204}Pb$ ratios in Kuriles volcanic rocks point to a reduced influence of sediment-derived fluids on a depleted MORB-type source mantle. Minor metasomatism of sub-arc mantle by fluids with a sedimentary spike is required to explain variations in B and Be systematics [6,9,43,52] and in Th/U, K/Cs and Rb/Cs ratios [12]. In detail, $^{87}Sr/^{86}Sr$ ratios down to 0.7028 in rear-arc volcanics point to normal levels of depletion in the underlying mantle, whereas the increasing $^{143}Nd/^{144}Nd$ ratios in volcanics closer to the fore arc [7] imply that their source was even more depleted and can be characterized as ultra-depleted [12]. Such an ultra-depleted mantle, with exceptionally low Pb isotopic ratios, allows the observed Pb isotopic ratios and their across-arc monotony to be explained by a small addition of sediment-derived fluids (see Fig. 7). At the same time, considerable fluid may have been released from the altered oceanic crust and this would be consistent with the observed combination of relatively high Sr isotope but low Pb isotope ratios, as well as high $\delta^{11}B$ values [9,44–46], in the fore-arc volcanics. In addition, the increase in Sr and Nd elemental concentrations toward the rear arc and slight decrease in Pb concentrations, coupled with the Sr, Nd and Pb isotopic ratios across-arc variations above, may also imply the gradual change of the dominant source for Sr, Nd and Pb elemental and isotopic source toward mantle-wedge-controlled (MORB-like).

Future work should aim to more precisely monitor these various elemental and isotopic parameters and needs to be carried out on samples from a narrowly defined, preferably more primitive stage of magmatic evolution. It is here demonstrated that anorthite megacrysts are useful for retrieving the chemistry of these early stages.

Acknowledgements

We are thankful to A.M. Davis for supervision of the ion microprobe analyses, O.N. Volynets for providing some samples of dredged basalts, Denton Ebel for help with the MELTS program, R. Frei for providing isotope analyses, L.V. Danyushevsky, J. Ryan, G. Yogodzinski and R. Sours-Page for helpful and exhaustive reviews. The Danish Natural Science Research Council (SNF) funded the INAA analyses (J.No. 11-5028), A.T. Anderson for INB support.

References

[1] J.B. Gill, Orogenic Andesites and Plate Tectonics, Springer Verlag, Berlin, 1981, 401 pp.
[2] Y. Tatsumi, Migration of fluid phase and genesis of basalt magma in subduction zones, J. Geophys.Res. 94 (1989) 4697–4707.
[3] V.I. Fedorchenko, A.I. Abdurakhmanov, R.I. Rodionova, Vulkanism Kuril'skoi ostrovnoi dugi: geologiya i petrogenesis (Volcanism of the Kurile Island Arc: geology and petrogenesis), Nauka, Moscow, 1989, 231 pp., in Russian.
[4] J.C. Bailey, T.I. Frolova, I.A. Burikova, Mineralogy, geochemistry and petrogenesis of Kurile island-arc basalts, Contrib. Mineral. Petrol. 102 (1989) 266–280.
[5] G.P. Avdeiko, O.N. Volynets, A.Yu. Antonov, A.A. Tsvetkov, Kurile island arc volcanism: structural and petrological aspects, Tectonophysics 199 (1991) 271–287.
[6] J.G. Ryan, J. Morris, F. Tera, W.P. Leeman, A.A. Tsvetkov, Cross-arc geochemical variations in the Kurile arc as a function of slab depth, Science 270 (1995) 625–627.
[7] D.Z. Zhuravlev, A.A. Tsvetkov, A.Z. Zhuravlev, N.G. Gladkov, I.V. Chernyshev, $^{143}Nd/^{144}Nd$ and $^{87}Sr/^{86}Sr$ ratios in recent magmatic rocks of the Kurile island arc, Chem. Geol. 66 (1987) 227–243.
[8] J.C. Bailey, O. Larsen, T.I. Frolova, Strontium isotope variations in lower Tertiary–Quaternary volcanic rocks from the Kurile island arc, Contrib. Mineral. Petrol. 95 (1987) 155–165.
[9] T. Ishikawa, F. Tera, Source, composition and distribution of fluid in the Kurile mantle wedge: constraints from across-arc variations of B/Nb and B isotopes, Earth Planet. Sci. Lett. 152 (1997) 123–138.
[10] I.N. Bindeman, T.I. Frolova, Redox conditions of formation of volcanic rocks of Kurile–Kamchatka island arc as a factor of across-arc geochemical zoning, Trans. Russian Acad. Sci. Earth Sci. Sect. 328 (1993) 490–493.
[11] K.F. Sergeev, M.L. Krasny (Eds.), Geology–Geophysical Atlas of the Kurile–Kamchatka Island System, Ministry of Geology of the USSR, Leningrad, 1987, 36 pp.
[12] J.C. Bailey, Role of subducted sediments in the genesis of Kurile–Kamchatka island arc basalts: Sr isotopic and elemental evidence, Geochim. J. 30 (1996) 289–321.
[13] T.K. Zlobin, Deep structure and geodynamics of the Kurile island arc, Yuzno–Sakhalinsk, 1989, 123 pp., in Russian.
[14] C.J. Nye, M.R. Reid, Geochemistry of primary and least fractionated lavas from Okmok Volcano, Central Aleutians: implications for arc magma genesis, J. Geophys. Res. 91 (1986) 10271–10287.
[15] S.M. Eggins, Origin and differentiation of picritic arc magmas, Ambae Aoba, Vanuatu, Contrib. Mineral. Petrol. 114 (1993) 79–100.
[16] Y. Panjasawatwong, L.V. Danyushevsky, A.J. Crawford, K.L. Harris, An experimental study of the effects of melt composition on plagioclase–melt equilibrium at 5 and 10 kbars: implications for the origin of magmatic high-An plagioclase, Contrib. Mineral Petrol. 118 (1995) 420–432.
[17] A.D. Johnson, D.S. Draper, Near-liquidus phase relations of an anhydrous high-magnesis basalt from the Aleutian islands: implications for arc magma genesis and ascent, J. Volcanol. Geotherm. Res. 52 (1992) 27–41.
[18] B.J. Giletti, Isotopic equilibrium/disequilibrium and diffusion kinetics in feldspars, in: Parsons, I. (Ed.), Feldspars and Their Reactions, 1994, pp. 351–382.
[19] B.J. Giletti, T.M. Shanahan, Alkali diffusion in plagioclase feldspar, Chem. Geol. 139 (1997) 3–20.
[20] D.J. Cherniak, E.B. Watson, A study of strontium diffusion in K-feldspar, Na–K feldspar and anorthite using Rutherford backscattering spectroscopy, Earth Planet. Sci. Lett. 113 (1992) 411–425.
[21] J.B. Brady, Diffusion data for silicate minerals, glasses, and liquids, in: Ahrens, T.J. (Ed.), Mineral Physics and Crystallography, A Handbook of Physical Constants, AGU Reference Shelf 2, 1995, pp. 269–290.
[22] O.N. Volynets, M.Yu. Khotin, Yu.M. Dubik, Olivine–anorthite inclusions of Kamchatka and Kurile volcanoes, in: Inclusions in the Volcanic Rocks of the Kurile–Kamchatka Island Arc, Nauka, Moscow, 1978, pp. 124–167, in Russian.
[23] T.I. Frolova, J.C. Bailey, I.A. Burikova, S.I. Dril', On genetic relatedness of low-silica olivine–anortite inclusions and host rocks of Kurile island arc, Pacif. Geol. 5 (1989) 27–35.
[24] M. Kimata, N. Nishida, M. Shimizu, S. Saito, T. Matsui, Y. Arakawa, Anorthite megacrysts from island arc basalts, Mineral. Magnet. 59 (1995) 1–14.
[25] R.J. Arculus, K.J.A. Wills, The petrology of plutonic blocks and inclusions from the Lesser Antilles island arc, J. Petrol. 21 (1980) 743–799.
[26] I.N. Bindeman, Volcanic eruptions produced by retrograde boiling of cumulates, Volcanol. Seismol. 13 (1992) 412–426.
[27] W.I. Rose Jr., A.T. Anderson Jr., L.G. Woodruff, S.B. Bonis, The October 1974 basaltic tephra from Fuego Volcano: description and history of the magma body, J. Volcanol. Geotherm. Res. 4 (1978) 3–53.
[28] L.V. Danyushevsky, M.R. Carrol, T.J. Falloon, Origin of high-An plagioclase in Tongan high-Ca boninites: implications for plagioclase–melt equilibria at low P_{H_2O}, Can. Mineral. 35 (1997) 313–326.

[29] R.L. Nielsen, J. Crum, R. Bourgeois, K. Haskall, L.M. Forsythe, M. Fisk, D.M. Christie, Melt inclusions in high-An plagioclase from the Gorda Ridge: an example of the local diversity of MORB parent magmas, Contrib. Mineral. Petrol. 122 (1995) 34–50.
[30] C. Siebe, C. Komorowskij, C. Navarro, J.F. McHone, H. Delgado, A. Cortes, Submarine eruption near Soccoro Island, Mexico; geochemistry and scanning electron microscopy studies of floating scoria and reticulite, J. Volcanol. Geotherm. Res. 68 (1995) 239–271.
[31] C.W. Sinton, D.M. Christie, V.L. Coombs, R.L. Nielsen, M.R. Fisk, Near primary melt inclusions in anorthite phenocrysts from the Galapagos Platform, Earth Planet. Sci. Lett. 119 (1993) 527–537.
[32] T.I. Frolova, P.Yu. Plechov, P.L. Tikhomirov, S.V. Churakov, Melt inclusions in minerals of olivine–anorthite enclaves of Kurile–Kamchatka island arc, Geokhimiya, 1999, in press.
[33] T.D. Housh, J.F. Luhr, Plagioclase–melt equilibria in hydrous systems, Amer. Mineral. 76 (1991) 477–492.
[34] H.-J. Yang, R.J. Kinzler, T.L. Grove, Experiments and models of anhydrous, basaltic olivine–plagioclase–augite saturated melts from 0.001 to 10 kbar, Contrib. Mineral. Petrol. 124 (1996) 1–18.
[35] M.S. Ghiorso, R.O. Sack, Chemical mass-transfer in magmatic processes, IV. A revised and internally consistent thermodynamic model for the interpolation and extrapolation of liquid–solid equilibria in magmatic systems at elevated temperatures and pressures, Contrib. Mineral. Petrol. 119 (1995) 197–212.
[36] R.W. Hinton, A.M. Davis, D.E. Scatena-Wachel, L. Grossman, R.J. Draus, A chemical and isotopic study of hibonite-rich refractory inclusions in primitive meteorites, Geochim. Cosmochim. Acta 52 (1988) 2573–2598.
[37] I.N. Bindeman, A.M. Davis, M.J. Drake, An ion microprobe study of plagioclase–basalt partition experiments at natural concentration levels of trace elements, Geochim. Cosmochim. Acta 62 (1998) 1175–1193.
[38] I.N. Bindeman, Magma mixing as a mechanism for the genesis of extrusive dacites of the Mendeleev Volcano, Kunashir Island, Kurile Islands, Pacific Geology (1990) 11–19.
[39] W.C. Phinney, Partition coefficients for iron between plagioclase and basalt as a function of oxygen fugacity; implication for Archean and lunar anorthosites, Geochim. Cosmochim. Acta 56 (1992) 1885–1895.
[40] J.H. Williamson, Least-squares fitting of a straight line, Can. J. Phys. 46 (1968) 1845–1854.
[41] M.J. Drake, The oxidation state of europium as an indicator of oxygen fugacity, Geochim. Cosmochim. Acta 39 (1975) 55–64.
[42] M.J. Drake, D.F. Weill, Partition of Sr, Ba, Eu^{2+}, Eu^{3+}, and other REE between plagioclase feldspar and magmatic liquid: an experimental study, Geochim. Cosmochim. Acta 39 (1975) 689–712.
[43] P.D. Noll Jr., H.E. Newsom, W.P. Leeman, J.G. Ryan, The role of hydrothermal fluids in the production of subduction zone magmas: evidence from siderophile and chalcophile trace elements and boron, Geochim. Cosmochim. Acta. 60 (1996) 587–611.
[44] D.M. Miller, S.L. Goldstein, C.H. Langmuir, Cerium/lead and lead isotope ratios in arc magmas and the enrichment of lead in the continents, Nature 368 (1994) 514–520.
[45] T. Ishikawa, E. Nakamura, Origin of the slab component in arc lavas from across-arc variation of B and Pb isotopes, Nature 370 (1994) 205–208.
[46] J.D. Morris, W.P. Leeman, F. Tera, The subducted component in island arc lavas: constraints from Be isotopes and B–Be systematics, Nature 344 (1990) 31–36.
[47] T. Shibata, E. Nakamura, Across–arc variations of isotope and trace element compositions from Quaternary basaltic volcanic rocks in northeastern Japan: implications for interaction between subducted oceanic slab and mantle wedge, J. Geophys. Res. 102 (1997) 8051–8064.
[48] W.M. White, A.W. Hofmann, H. Puchelt, Isotope geochemistry of Pacific Mid-Ocean ridge basalt, J. Geophys. Res. 92 (1987) 4881–4893.
[49] H. Keppler, Constraints from partitioning experiments on the composition of subduction-zone fluids, Nature 380 (1996) 237–240.
[50] Y. Tatsumi, T. Kosigo, Trace element transport during dehydration processes in the subducted oceanic crust: 2. Origin of chemical and physical characteristics in arc magmatism, Earth Planet. Sci. Lett. 148 (1997) 207–221.
[51] E. Stolper, S. Newman, The role of water in the petrogenesis of Mariana trough magmas, Earth Planet. Sci. Lett. 121 (1994) 293–325.
[52] A.A. Tsvetkov, O.N. Volynets, First data on ^{10}Be in recent volcanics of the Kurile–Kamchatka island arc system in relation to sediment subduction, Isotopenpraxis 26 (1990) 603–607.